

Deep Unfolding of Iteratively Reweighted ADMM for Wireless RF Sensing

Udaya S.K.P. Miriya Thantrige, Peter Jung, and Aydin Sezgin

Abstract—We address the detection of material defects, which are inside a layered material structure using compressive sensing based multiple-input and multiple-output (MIMO) wireless radar. Here, the strong clutter due to the reflection of the layered structure’s surface often makes the detection of the defects challenging. Thus, sophisticated signal separation methods are required for improved defect detection. In many scenarios, the number of defects that we are interested in is limited and the signaling response of the layered structure can be modeled as a low-rank structure. Therefore, we propose joint rank and sparsity minimization for defect detection. In particular, we propose a non-convex approach based on the iteratively reweighted nuclear and ℓ_1 -norm (a double-reweighted approach) to obtain a higher accuracy compared to the conventional nuclear norm and ℓ_1 -norm minimization. To this end, an iterative algorithm is designed to estimate the low-rank and sparse contributions. Further, we propose deep learning to learn the parameters of the algorithm (i.e., algorithm unfolding) to improve the accuracy and the speed of convergence of the algorithm. Our numerical results show that the proposed approach outperforms the conventional approaches in terms of mean squared errors of the recovered low-rank and sparse components and the speed of convergence.

Index Terms—Algorithm unfolding, Clutter suppression, Defects detection, Compressive sensing, Reweighted norm

I. INTRODUCTION

NON-destructive testing (NDT) is important in many areas such as remote sensing, security, and many more [1]–[3]. Further, NDT plays an important role in many industrial applications because it does not cause damage to the material under test. The electromagnetic (EM) waves-based remote sensing has many potential applications such as behind the wall object identification [4], multi-layer target detection [5], material characterization [6], defect detection [3], [7]–[9] and many more. In EM waves-based detection of objects/defects which are behind or inside a layered structure, the EM waves that reflect from the object/defect are analyzed. Here, one

The work of U. S. K. P. M. Thantrige and A. Sezgin is funded by the Deutsche Forschungsgemeinschaft (DFG, German Research Foundation) Project-ID287022738 TRR 196 (S02) and the work of P. Jung is funded by the German Federal Ministry of Education and Research (BMBF) in the framework of the international future AI lab “AI4EO—Artificial Intelligence for Earth Observation: Reasoning, Uncertainties, Ethics and Beyond” (Grant number: 01DD20001).

U. S. K. P. M. Thantrige and A. Sezgin are with the Institute of Digital Communication Systems (DCS), Ruhr University Bochum (RUB), 44801 Bochum, Germany. Email: {udaya.miriyathantrige, aydin.sezgin}@rub.de.

P. Jung is with the Institute of Communications and Information Theory, Technical University Berlin, 10587 Berlin, Germany and Data Science in Earth Observation, Technical University of Munich, 82024 Taufkirchen/Ottobrunn, Germany. Email: peter.jung@tu-berlin.de.

major challenge is the presence of strong unwanted reflections, i.e., clutter [4], [10]. In the EM waves-based defect detection, the main source of the clutter is the reflection from the surface of the layered material structure.

The state-of-the-art clutter suppression methods such as background subtraction (BS) and subspace projection (SP) [11] are not able to suppress the clutter in the context of object/defect detection. This is due to the fact in the BS requires the reference data of the scene and this reference data is not available most of the time. Moreover, in the SP prior knowledge is required to determine the perfect threshold for clutter removal. Further, clutter suppression becomes even more challenging if objects and clutter are closely located. This occurs regularly in the detection of defects which are inside a layered structure. Then, due to the small delay spread between the signaling responses of defects and clutter superimpose each other. In order to overcome these challenges, advanced signal processing methods are required for clutter suppression.

Note that, in many scenarios, the number of defects is limited. Therefore, the signaling response of the defect is sparse in nature. By exploring this, compressive sensing (CS) [12] based approaches have shown promising results in object/defect detection with clutter [4], [10]. Also, the CS-based approaches do not require full measurement data set, which results in fast data acquisition and less sensitivity to sensor failure, wireless interference and jamming. In CS based approaches, it is considered that the clutter resides in a low-rank subspace and the response of the objects is sparse [4], [10]. To this end, for the general data acquisition model the received data vector $\mathbf{y} \in \mathbb{C}^K$ is modelled as a combination of low-rank matrix $\mathbf{L} \in \mathbb{C}^{M \times N}$ and a sparse matrix $\mathbf{S} \in \mathbb{C}^{M \times N}$ with $M \leq N$

$$\mathbf{y} = \mathbf{A}_l \text{vec}(\mathbf{L}) + \mathbf{A}_s \text{vec}(\mathbf{S}) + \mathbf{n}. \quad (1)$$

Here, $\mathbf{A}_l, \mathbf{A}_s \in \mathbb{C}^{K \times MN}$ with $K \ll MN$, $\mathbf{n} \in \mathbb{C}^K$ are compression operators and measurement noise, respectively. Further, $\text{vec}(\cdot)$ denotes the vectorization operator, which converts a matrix to a vector by stacking the columns of the matrix. Given the received data vector \mathbf{y} our aim to estimate the signals of interest (\mathbf{L} and \mathbf{S}) using a few number of linear measurement. In this problem, the compression ratio is defined as K/MN . Note that the above problem is also known as robust principal component analysis (RPCA) [13]. The problem given in (1) has different types (a) Standard/classical RPCA in which both \mathbf{A}_l and \mathbf{A}_s in (1) are identity matrices [13], (b) The matrices $\mathbf{A}_l = \mathbf{A}_s = \mathbf{A}$ and \mathbf{A} is a selection

operator which selects a random subset of size K from MN entries [14], (c) Both \mathbf{A}_l and \mathbf{A}_s are linear operators which map the vector space MN to the vector space K [14]. In this work, we focus on (c) and we consider two cases where $\mathbf{A}_l = \mathbf{A}_s = \mathbf{A}$ and $\mathbf{A}_l \neq \mathbf{A}_s$. Estimating a matrix with the lowest rank and the sparsest matrix from the compressed observations are NP-hard problems and thus difficult to solve. To this end, convex relaxations of sparsity (ℓ_0 -norm: the number of nonzero components) and rank in terms of ℓ_1 -norm of a matrix (absolute sum of elements) and nuclear norm of a matrix (sum of singular values of a matrix) are utilized, respectively [15]–[17].

Next, we briefly discuss the recovery guarantees of the RPCA problem. Here, we focus on the standard RPCA problem i.e., both \mathbf{A}_l and \mathbf{A}_s in (1) are identity matrices. We consider above scenario because it is well studied in the literature and well understood. So we briefly discuss when the separation of low-rank matrix \mathbf{L} and sparse matrix \mathbf{S} is possible. Based on [13], if \mathbf{L} is sufficiently low-rank but not sparse and \mathbf{S} is sufficiently sparse but not low-rank, the matrices \mathbf{L} and \mathbf{S} can be estimated exactly with a high probability of success. Here, to solve the RPCA problem convex relaxations of sparsity and rank in terms of ℓ_1 -norm of a matrix and nuclear norm of a matrix are utilized [13]. Let $\bar{K} = \max(N, M)$, $K = \min(N, M)$ and positive constants c_o , p_s and p_r . We consider the following theorem from [13].

Theorem 1: It is possible to recover \mathbf{L} and \mathbf{S} with a probability at least $1 - c\bar{K}^{-10}$ when $\text{rank}(\mathbf{L}) \leq p_r K(\mu)^{-1}(\log(\bar{K}))^{-1}$ and $\|\mathbf{S}\|_0 \leq p_s \bar{K} K$.

Here, μ is the incoherence condition parameter of the low-rank matrix \mathbf{L} as defined in [13]. As discussed in [18]–[20] when the incoherence condition parameter μ is small, the singular value vector of the matrix \mathbf{L} is spread out. The main message of Theorem 1 is that to recover the \mathbf{L} and \mathbf{S} successfully, the rank of the matrix \mathbf{L} should not be too large and the matrix \mathbf{S} should be reasonably sparse. That means that the rank of the matrix \mathbf{L} and sparsity of the matrix \mathbf{S} is bounded.

To this end, we have shortly discussed when the separation of low-rank and sparse matrices make sense. Next, we shortly discuss what is the lowest possible mean squared error of the low-rank and sparse matrix recovery that can be achieved. For that we have chosen the Cramér–Rao bound (CRB) analysis of the RPCA given in [14]. For RPCA problem with $\mathbf{A}_l = \mathbf{A}_s = \mathbf{A}$ in (1), the CRB of unbiased estimation for \mathbf{L} and \mathbf{S} is derived in [14]. Here, similar to [13], the RPCA problem is solved using the ℓ_1 -norm and nuclear norm minimization. To this end, let the estimated low-rank and sparse matrices be given by $\hat{\mathbf{L}}$ and $\hat{\mathbf{S}}$, respectively. Now, similar to Theorem 1, it is assumed that the rank of the matrix \mathbf{L} and the sparsity of the matrix \mathbf{S} is bounded as given below.

$$\begin{aligned} \text{rank}(\mathbf{L}) = r &\leq l, \\ \|\mathbf{S}\|_0 &\leq s. \end{aligned} \quad (2)$$

Here, l and s are positive constants. Let the received data vector \mathbf{y} in (1) follows $\mathbf{y} \sim \mathcal{N}(\text{Avec}(\mathbf{L} + \mathbf{S}), \sigma^2 \mathbf{I}_K)$. Now,

CRB of unbiased estimation for \mathbf{L} and \mathbf{S} is bounded by¹

$$\begin{aligned} \left\{ s - N_0 + \frac{1}{3} \frac{KN_0}{K-s} + \frac{2}{3} \frac{MNN_0}{K-s} \right\} \sigma^2 \leq \text{CRB}(\mathbf{L}, \mathbf{S}) \leq \\ \left\{ s - N_0 + \frac{3KN_0}{K-s} + \frac{2MNN_0}{K-s} \right\} \sigma^2. \end{aligned} \quad (3)$$

Here, \mathbf{I}_K is the identity matrix with a dimension of $K \times K$ and $N_0 = (M + N)r - r^2$.

Next, we are going to discuss the disadvantages of convex relaxation of RPCA and the alternative approaches instead of the convex relaxation. In general, the ℓ_1 -norm minimization and the ℓ_0 -norm minimization have different solutions. Further, the ℓ_1 -norm minimization is a loose approximation of the ℓ_0 -norm minimization. Due to this reason, alternative approaches such as the weighted ℓ_1 -norm minimization have been considered for improved performance over the ℓ_1 -norm minimization [21].

Note that in many applications, the important properties are preserved by the large coefficients/singular values of the signal. However, the ℓ_1 -norm/nuclear norm minimization algorithms shrink all the coefficients/singular values with the same threshold. Thus, to avoid this weakness, we should shrink less the larger coefficients/singular values. Therefore, in both ℓ_1 -norm and nuclear norm minimization, the weighted ℓ_1 -norm and weighted nuclear norm minimization have been considered [21]–[23]. Note that, the non-convex approaches, i.e., reweighted nuclear norm and ℓ_1 -norm minimization have shown better performance over the convex relaxations by providing tighter characterizations of rank and sparsity. For instance, studies [21], [24] have shown that the reweighted ℓ_1 -norm minimization outperforms the ℓ_1 -norm minimization. Similarly, studies [22], [23] have shown that the reweighted nuclear norm outperforms the nuclear norm minimization. Although reweighted approached like the reweighted ℓ_1 -norm minimization outperforms the convex ℓ_1 -norm minimization, still the reweighted ℓ_1 -norm minimization and their convergence has not been fully studied [25].

To this end, we formulate an optimization problem based on the reweighted nuclear norm and reweighted ℓ_1 -norm minimization to jointly estimate the low-rank matrix and the sparse vector from few compressive measurements. Note that our iterative algorithm is based on the alternating direction method of multipliers (ADMM) [26]. Then, the estimated sparse vector is used to identify defects. To the best of our knowledge, the full doubly-reweighted approach, i.e., wrt. nuclear norm and ℓ_1 -norm has not yet been studied in the literature for the compressive case.

In iterative algorithms, the accuracy of the recovered signal component and the convergence rate depends on the proper selection of parameters (e.g., regularization/thresholding/denoising parameters). Generally, parameters are chosen by handcrafting, and it is a time-consuming task. In this context, machine learning-based parameter learning using the training data has shown promising results in many applications

¹Here, \mathbf{A} is assumed to be a selection operator which selects a random subset of size K from MN entries. Since this is closest matching CRB to our model given in (1), we have considered this formulation as a benchmark.

such as sparse vector recovery [27]–[29] and image processing [30]. This approach is known as algorithm unrolling/unfolding. An interesting overview of the algorithm unfolding can be found in [31]. The authors in [27] unfolded the iterative shrinkage and thresholding algorithm (ISTA). It is called as learned ISTA (LISTA) and the LISTA converges twenty times faster than the ISTA.

In this work, we propose deep learning-based parameter learning to improve the accuracies of the recovered low-rank and sparse components and the convergence rate of the ADMM based iterative algorithm. In the following, we emphasize the differences of our approach with the existing low-rank plus sparse recovery approaches. Most of the work in the literature focus on the standard RPCA where both \mathbf{A}_l and \mathbf{A}_s in (1) to be identity matrices [23], [32]. Further, most of the time RPCA problems are solved by using the convex relaxation, i.e., nuclear norm and ℓ_1 -norm minimization or with the single reweighting, i.e., either reweighted ℓ_1 -norm or reweighted nuclear norm [23], [32]–[34]. In this work, we study the joint reweighted nuclear norm and reweighted ℓ_1 -norm (full doubly-reweighted) compressive sensing data acquisition model. In the context of the algorithm unfolding for the RPCA, the convolutional robust principal component analysis (CORONA) [33] and [34] are the closest work to our work. There are fundamental differences between our work and [33], [34]. (a) Our methodology is fundamentally different from the methodology that both [33], [34] have used to solve the RPCA. In more details, both [33], [34] considered the standard convex relaxation ($\ell_{1,2}$ -norm and nuclear norm) to solve the RPCA problem, while we propose the reweighted ℓ_1 -norm and reweighted nuclear norm.

Further, our iterative algorithm to solve RPCA is based on ADMM while iterative algorithm in [33], [34] based on fast ISTA (FISTA). The motivation to propose ADMM over ISTA/FISTA for RPCA is as follows. As shown in [13], [35] for RPCA, the ADMM based approach is able to achieve the desired solution with a good recovery error with a small number of iteration for a wide range of applications. Also, it is shown that ADMM converges faster than ISTA/FISTA. As an example for ℓ_1 -norm minimization, in [36] it is shown that the ADMM achieves the desired solution with fewer iterations than ISTA/FISTA. (b) Different from [33], [34] our focus is on defect detection based on the stepped-frequency continuous (SFCW) radar while [33], [34] focus on ultrasound imaging application. Further, measurement data of [33], [34] have considered that both \mathbf{A}_l and \mathbf{A}_s in (1) are identity matrices. However, in this work, we consider the joint reweighted nuclear norm and reweighted ℓ_1 -norm (full doubly-reweighted) with a compressive sensing data acquisition model i.e., both \mathbf{A}_l and \mathbf{A}_s in (1) are not identity matrices. Further, we have studied the performance of our approach with a generic real-value Gaussian model and a complex-valued SFCW radar model for different compression ratios.

In addition to that, CORONA is based on a convolutional neural network while our approach is based on a dense neural network. The main motivation to prefer a dense neural network over a convolutional neural network is that the system model of the defect detection based on the SFCW radar

does not include the convolutional operation. Therefore, we consider a dense DNN which match to our system model more than the convolutional DNN. In addition to that in the compressive sensing data acquisition model, the received data vector \mathbf{y} in (1) has a much lower dimension than the low-rank and sparse matrices \mathbf{L} and \mathbf{S} i.e., $K \ll MN$. In the estimation of \mathbf{L} and \mathbf{S} from \mathbf{y} , lower dimension to higher dimension mapping is required. Here, we experience that the performance of the convolution DNN is limited. This is due to the fact that, as the compression ratio increases more zero padding is required. Another advantage of the dense DNN is the simplicity of initialization of the weights of the DNN. Here, it is possible to initialize the weights of the DNN by using the measurement matrices \mathbf{A}_l and \mathbf{A}_s . Also, for some applications, there is no such requirement to train the weights of the DNN that are initialized based on the measurement matrices. Here, only training the parameters of the iterative algorithm is sufficient to get an improved performance. However, with a convolution DNN this may not be straightforward as a dense DNN. Because finding a relationship between the measurement matrices and the weights of the convolutional DNN is not straightforward.

Also, in CORONA [33], a custom complex-valued convolution layers and singular value decomposition operations are utilized. Note that in our work, we have implemented a dense DNN which supports complex-valued data in linear layers and singular value decomposition (SVD) operation.

A. Contribution

The contributions of this work are summarized as follows:

- We propose the non-convex fully double-reweighted approach i.e., both reweighted ℓ_1 -norm and reweighted nuclear norm simultaneously to solve the RPCA problem in the compressive sensing data acquisition model which reflects more the practical problem at hand.
- We propose an iterative algorithm based on ADMM to estimate the low-rank and sparse components jointly.
- We propose a deep neural network (DNN) to learn the parameters of the iterative algorithm (i.e., algorithm unfolding) from the training data.
- We consider two types of data to evaluate our approach. As a practical application, the defect detection by SFCW radar from compressive measurements with $\mathbf{A}_l \neq \mathbf{A}_s$ is used. In addition to that, for a standard benchmark, a generic Gaussian data acquisition model with $\mathbf{A}_l = \mathbf{A}_s = \mathbf{A}$ is used. Further, we compare the performance of the proposed DNN based approach with the standard convex approach (i.e., nuclear norm and ℓ_1 -norm minimization) and the untrained ADMM based iterative algorithm for different compression ratios. In both cases, our numerical results show that the proposed approach outperforms the conventional approaches in terms of mean squared errors of the recovered low-rank and sparse components and the speed of convergence.

The remainder of the paper is organized as follows. We introduce the SFCW radar-based defect detection and the low-rank plus sparse recovery with reweighting in Section II. In

Section III we discuss the DNN-based low-rank plus sparse recovery algorithm unfolding. In Section IV, we provide an evaluation of the proposed DNN-based low-rank plus sparse recovery algorithm unfolding approaches and provide interesting insights. Section V concludes the paper.

II. SYSTEM MODEL

First, we briefly present the system model of the mono-static SFCW radar-based defect detection. Next, we are going to discuss the ADMM based iterative algorithm for the low-rank plus sparse recovery.

A. SFCW radar based defect detection

We consider a SFCW radar with M transceivers which are placed in parallel to the single-layered material structure while maintaining an equal distance between transceivers as shown in Fig. 1. In SFCW radar, each transceiver transmits a stepped-frequency signal containing N frequencies which are equally spaced over the bandwidth of B Hz. To this end, the received signal corresponding to all M transceivers and N frequencies $\mathbf{Y} \in \mathbb{C}^{M \times N}$ are given by

$$\mathbf{Y} = \mathbf{Y}^l + \mathbf{Y}^d + \mathbf{Z}. \quad (4)$$

Note that, \mathbf{Y} consists of two main components, the reflection of the layered material structure (\mathbf{Y}^l) and the reflection of the defects (\mathbf{Y}^d). Here, \mathbf{Z} is the additive Gaussian noise matrix. Next, we discuss in details the modeling of the received signal of the defects by using the propagation time delay. To this end, the scene shown in Fig. 1 is hypothetically partitioned into a rectangular grid of size Q . Suppose that the round-travel time of the signal from the m -th antenna location to the p -th defect and back is given by $\tau_{m,p}$. Then, the received signal of the defects in m -th transceiver corresponding to n -th frequency band (f_n) $y_{m,n}^d$ is given by

$$y_{m,n}^d = \sum_{p=1}^P \alpha_p \exp(-j2\pi f_n \tau_{m,p}). \quad (5)$$

Here, $j = \sqrt{-1}$, $\alpha_p \in \mathbb{C}$ is the complex signal strength of the p -th defect and P is the total number of defects. To this end, $\text{vec}(\mathbf{Y}^d) \in \mathbb{C}^{MN \times 1}$ is given by $\text{vec}(\mathbf{Y}^d) = \mathbf{D}\mathbf{s}$, where vector $\mathbf{s} \in \mathbb{C}^{Q \times 1}$ contains all the α_p values of the defects. Since there are P defects, the vector \mathbf{s} only contains P non-zero entries. The matrix \mathbf{D} is given by $[(\mathbf{D}_1)^T, \dots, (\mathbf{D}_m)^T, \dots, (\mathbf{D}_M)^T]^T \in \mathbb{C}^{MN \times Q}$. Note that, the (n, q) -th element of the matrix $\mathbf{D}_m \in \mathbb{C}^{N \times Q}$ is given by $\exp(-j2\pi f_n \tau_{m,q})$, where $\tau_{m,q}$ is the propagation time delay between the m -th antenna to the q -th grid location. Note that, we assume that the propagation time delays of the defects are exactly matched with the propagation time delays of the grid locations.

B. Compressed sensing (CS) approach

In the compressed sensing (CS) setup only a subset of antennas/frequencies are available or selected. Now, the reduced data vector $\mathbf{y}_{cs} \in \mathbb{C}^{K \times 1}$ of size $K (\ll MN)$ is given by

$$\mathbf{y}_{cs} = \Phi(\text{vec}(\mathbf{Y})) = \Phi \text{vec}(\mathbf{Y}^l) + \Phi \mathbf{D}\mathbf{s} + \Phi \text{vec}(\mathbf{Z}), \quad (6)$$

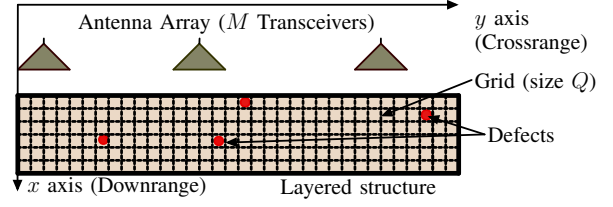


Fig. 1. Getting the measurements of a single-layered material structure using a SFCW radar with M transceivers.

where $\Phi \in \mathbb{R}^{K \times MN}$ is the selection matrix. The matrix Φ has a single non-zero element of value 1 in each row to indicate the selected frequency of a particular antenna if that antenna is selected. Here, our main objective is to recover \mathbf{Y}^l and \mathbf{s} from the reduced data vector \mathbf{y}_{cs} using the low-rank plus sparse recovery approach as detailed below.

C. Low-rank-plus-sparse recovery algorithm

From now on we consider the general data acquisition model given in (1) in Section I i.e., $\mathbf{y} = \mathbf{A}_l \text{vec}(\mathbf{L}) + \mathbf{A}_s \text{vec}(\mathbf{S}) + \mathbf{n}$. Note that, the SFCW radar model given in (6) is mapped to the generic measurement model by considering $\mathbf{A}_s = \Phi \mathbf{D}$, $\mathbf{A}_l = \Phi$, $\mathbf{Y}^l = \mathbf{L}$, $\mathbf{s} = \text{vec}(\mathbf{S})$ and $\mathbf{y}_{cs} = \mathbf{y}$, respectively. Our objective is to recover the low-rank matrix \mathbf{L} and the sparse matrix \mathbf{S} from the compressive measurements \mathbf{y} . Thus, the estimation of \mathbf{L} and \mathbf{S} from \mathbf{y} is done by minimizing rank and the sparsity (ℓ_0 -norm). Note that, rank and ℓ_0 -norm minimization problems are usually NP-hard. Thus, one may use convex relaxations based on the nuclear norm of a matrix and ℓ_1 -norm of a matrix as follows

$$\begin{aligned} \{\hat{\mathbf{L}}, \hat{\mathbf{S}}\} &= \arg \min_{\mathbf{L}, \mathbf{S}} \lambda_l \|\mathbf{L}\|_* + \lambda_s \|\mathbf{S}\|_1, \\ \text{s.t. } \|\mathbf{y} - \mathbf{A}_s \text{vec}(\mathbf{S}) - \mathbf{A}_l \text{vec}(\mathbf{L})\|_2^2 &\leq \epsilon. \end{aligned} \quad (7)$$

Here, λ_l , λ_s are regularization parameters and ϵ is a small positive constant (noise bound). Further, $\|\cdot\|_1$, $\|\cdot\|_*$ are the ℓ_1 -norm and nuclear norm of a matrix, respectively. The resulting convex problems, i.e., ℓ_1 -norm and nuclear norm minimization are well studied in the literature and there are several non-convex approaches to improve over the standard convex relaxation. One well-known approach is iterative reweighting of the ℓ_1 -norm [21], [28], [37] and nuclear norm [23], [38]–[40]. Alternating direction method of multipliers (ADMM) is used to solve the problem given in (7) [26]. First, we formulate the problem given in (7) based on the ADMM approach, and then we introduce the non-convex double-reweighted approach i.e., both reweighted ℓ_1 -norm and reweighted nuclear norm simultaneously. Let the signal component value of \mathbf{S} and \mathbf{L} at the t -th iteration be denoted as \cdot^t . Now, based on the ADMM \mathbf{S} and \mathbf{L} are estimated by

$$\begin{aligned} \mathbf{L}^{t+1} &= \arg \min_{\mathbf{L}} \lambda_l \|\mathbf{L}\|_* + \\ &\frac{\rho}{2} \left\| \mathbf{A}_s \text{vec}(\mathbf{S}^t) + \mathbf{A}_l \text{vec}(\mathbf{L}) - \mathbf{y} + \frac{1}{\rho} \mathbf{u}^t \right\|_2^2, \end{aligned} \quad (8)$$

$$\mathbf{S}^{t+1} = \arg \min_{\mathbf{S}} \lambda_s \|\mathbf{S}\|_1 + \frac{\rho}{2} \left\| \mathbf{A}_s \text{vec}(\mathbf{S}) + \mathbf{A}_l \text{vec}(\mathbf{L}^{t+1}) - \mathbf{y} + \frac{1}{\rho} \mathbf{u}^t \right\|_2^2 \quad (9)$$

$$\mathbf{u}^{t+1} = \mathbf{u}^t + \rho (\mathbf{A}_s \text{vec}(\mathbf{S}^{t+1}) + \mathbf{A}_l \text{vec}(\mathbf{L}^{t+1}) - \mathbf{y}). \quad (10)$$

Here, $\mathbf{u}, \rho > 0$ are auxiliary variables and a penalty factor. Let $\boldsymbol{\sigma}(\mathbf{L}) = [\sigma_1, \dots, \sigma_m, \dots, \sigma_M] \in \mathbb{R}^M$ be the singular values of the matrix \mathbf{L} . Now, nuclear norm of the matrix \mathbf{L} is given by $\|\mathbf{L}\|_* = \|\boldsymbol{\sigma}(\mathbf{L})\|_1$. Now, we are going to introduce the weighted ℓ_1 -norm and weighted nuclear norm to the sub-problems given in (8) and (9) as follows.

$$\mathbf{L}^{t+1} = \arg \min_{\mathbf{L}} \lambda_l \|\mathbf{w}_l^t \odot \boldsymbol{\sigma}(\mathbf{L})\|_1 + \frac{\rho}{2} \left\| \mathbf{A}_s \text{vec}(\mathbf{S}^t) + \mathbf{A}_l \text{vec}(\mathbf{L}) - \mathbf{y} + \frac{1}{\rho} \mathbf{u}^t \right\|_2^2 \quad (11)$$

$$\mathbf{S}^{t+1} = \arg \min_{\mathbf{S}} \lambda_s \|\mathbf{w}_s^t \odot \mathbf{S}\|_1 + \frac{\rho}{2} \left\| \mathbf{A}_s \text{vec}(\mathbf{S}) + \mathbf{A}_l \text{vec}(\mathbf{L}^{t+1}) - \mathbf{y} + \frac{1}{\rho} \mathbf{u}^t \right\|_2^2. \quad (12)$$

The operator \odot denotes element-wise multiplication. Here, $\mathbf{w}_l^t \in \mathbb{R}^M$ and $\mathbf{w}_s^t \in \mathbb{R}^{MN}$ are non-negative weight vectors. To this end, \mathbf{w}_l^t and \mathbf{w}_s^t are calculated based on the previous estimation of the \mathbf{L} and \mathbf{S} i.e., \mathbf{L}^t and \mathbf{S}^t .

$$\mathbf{w}_l^t = g_l(\boldsymbol{\sigma}(\mathbf{L}^t)) \quad \text{and} \quad \mathbf{w}_s^t = g_s(|\mathbf{S}^t|). \quad (13)$$

Here, $g_l(\cdot)$ and $g_s(\cdot)$ are the decay functions which are used to calculate the weights. There are several decay functions are proposed in the literature and an overview of many known decay functions for the nuclear norm is given in [40]. In this work, we consider the element-wise soft-thresholding [28] and element-wise singular value soft-thresholding (i.e., element-wise soft-thresholding on the singular value of a matrix) [41] as proximal operators of weighted ℓ_1 -norm and weighted nuclear norm, respectively. Now, \mathbf{L}^{t+1} and \mathbf{S}^{t+1} are given by

$$\mathbf{L}^{t+1} = \text{SVT}_{\lambda_{LT}} \left(\mathbf{A}_l^* \left(\mathbf{y} - \mathbf{A}_s \text{vec}(\mathbf{S}^t) + \frac{\mathbf{u}^t}{\rho} \right) \right), \quad (14)$$

$$\mathbf{S}^{t+1} = \text{ST}_{\lambda_{ST}} \left(\mathbf{A}_s^* \left(\mathbf{y} - \mathbf{A}_l \text{vec}(\mathbf{L}^{t+1}) + \frac{\mathbf{u}^t}{\rho} \right) \right), \quad (15)$$

where $\text{SVT}(\cdot)$ and $\text{ST}(\cdot)$ are the element-wise singular value soft-thresholding and element-wise soft-thresholding operators [28], [41], respectively. Note that, $(\cdot)^*$ is a linear operator which back project the vector in to the target matrix subspace. There are two options for $(\cdot)^*$. (a) Hermitian transpose $(\cdot)^H$ as done in [28]. (b) Moore–Penrose pseudo inverse $(\cdot)^\dagger$ as done in [4]. Next, we are going to discuss the element-wise soft-thresholding in more details.

D. Element-wise soft-thresholding and singular value soft-thresholding

Consider (15) and let the intermediate value in the $t+1$ -th iteration as $\mathbf{S}_I^{t+1} \in \mathbb{C}^{M \times N}$ before the soft-thresholding be given by

$$\mathbf{S}_I^{t+1} = \mathbf{A}_s^* \left(\mathbf{y} - \mathbf{A}_l \text{vec}(\mathbf{L}^{t+1}) + \frac{1}{\rho} (\mathbf{u})^t \right). \quad (16)$$

To estimate the sparse component in the $t+1$ -th iteration \mathbf{S}^{t+1} , element-wise soft-thresholding is applied to each element of the matrix \mathbf{S}_I^{t+1} individually. To this end, the element-wise soft-thresholding operation of the m -th row and n -th column element of the matrix \mathbf{S}_I^{t+1} is defined as ²

$$\text{ST}_{\lambda_{ST}^{m,n}}(s_{m,n}^{t+1}) = \exp(j\theta) \max(|s_{m,n}^{t+1}| - \lambda_{ST}^{m,n}, 0). \quad (17)$$

Here, θ is the phase angle of the $s_{m,n}^{t+1}$ in radians. Here, $\lambda_{ST}^{m,n}$ is the threshold value related to the element $s_{m,n}^{t+1}$. Note that the threshold values $(\lambda_{ST}^{m,n} \forall m, n)$ change from iteration to iteration. However, for better readability, we not include the index t . Here, a decay function is used to calculate the threshold value. In this work, we consider the common log-determinant heuristic [21] and exponential decay [38], [40] as decay functions. To this end, the log-determinant heuristic decay function is given by

$$g_s(x) = g_{\log}(x) = \frac{1}{x + \gamma}. \quad (18)$$

Similarly, the exponential heuristic decay function is given by

$$g_s(x) = g_{\exp}(x) = \frac{1}{\gamma} \exp\left(\frac{-x}{\gamma}\right). \quad (19)$$

Here, γ is a positive constant. To this end, the estimation of matrix \mathbf{S} in $t+1$ -th iteration, i.e., \mathbf{S}^{t+1} is given by

$$\mathbf{S}^{t+1} = \text{ST}_{\lambda_{ST}^t}(\mathbf{S}_I^{t+1}), \quad (20)$$

where $\lambda_{ST}^t = [\lambda_{ST}^{1,1}, \dots, \lambda_{ST}^{m,n}, \dots, \lambda_{ST}^{M,N}]$ contains different threshold values for each element of \mathbf{S} for the $t+1$ -th iteration. These threshold values are derived based on the previous estimate of \mathbf{S} , i.e., \mathbf{S}^t . Thus, $\lambda_{ST}^{m,n}$ is given by

$$\lambda_{ST}^{m,n} = \lambda_S g_s(|s_{m,n}^t|). \quad (21)$$

Here λ_S is a positive constant and $s_{m,n}^t$ is the m -th row and n -th column element of the t -th estimation of the sparse component (\mathbf{S}^t). The same concept is also applied to the singular value soft-thresholding which is used to solve the problem given in (14) as discussed next. In this work, we consider the same decay function for both sparsity and rank, i.e., $g_s(\cdot) = g_l(\cdot)$. First, consider (14) and let the intermediate value in $t+1$ -th iteration, $\mathbf{L}_I^{t+1} \in \mathbb{C}^{M \times N}$ before applying the singular value soft-thresholding be given by

$$\mathbf{L}_I^{t+1} = \mathbf{A}_l^* \left(\mathbf{y} - \mathbf{A}_s \text{vec}(\mathbf{S}^t) + \frac{1}{\rho} (\mathbf{u})^t \right). \quad (22)$$

The singular value decomposition (SVD) of the matrix $\mathbf{L}_I^{t+1} \in \mathbb{C}^{M \times N}$ with $M \leq N$ is given as $\mathbf{L}_I^{t+1} = \mathbf{U} \boldsymbol{\Lambda} \mathbf{V}^T$. Here, $\mathbf{U} \in \mathbb{C}^{M \times M}$ and $\mathbf{V} \in \mathbb{C}^{N \times N}$ are the matrices of left and right singular vectors. $\boldsymbol{\Lambda} \in \mathbb{R}^{M \times N}$ is a rectangular diagonal matrix with $\boldsymbol{\sigma}(\mathbf{L}_I^{t+1}) = [\sigma_1, \dots, \sigma_m, \dots, \sigma_M]$ on the diagonal and zeros elsewhere. Next, the element-wise singular value soft-thresholding is applied to the singular values of the matrix \mathbf{L}_I^{t+1} to estimate the \mathbf{L}^{t+1}

$$\begin{aligned} \mathbf{L}^{t+1} &= \text{SVT}_{\lambda_{LT}^t}(\mathbf{L}_I^{t+1}), \\ &= \mathbf{U} \text{diag}\left(\text{ST}_{\lambda_{LT}^t}(\boldsymbol{\sigma}(\mathbf{L}_I^{t+1}))\right) \mathbf{V}^T. \end{aligned} \quad (23)$$

²Note that, here we consider the complex-version of the soft-thresholding.

Note that, here $\text{ST}_{\lambda_{LT}^t}(\cdot)$ is the element-wise soft-thresholding operator and the operator $\text{diag}(\cdot)$ takes a vector as an input and returns a square diagonal matrix in which the main diagonal contains the vector elements and zeros elsewhere. Here, $\lambda_{LT}^t = [\lambda_{LT}^1, \dots, \lambda_{LT}^m, \dots, \lambda_{LT}^M]$ contains the different threshold values and λ_{LT}^m is calculated based on the singular values of the previous estimate of matrix L as given below.

$$\lambda_{LT}^m = \lambda_L g_l(\sigma_m^t). \quad (24)$$

Here, σ_m^t is the m -th singular value of the L^t and λ_L is a positive constant.

Algorithm 1: Low-rank-plus-sparse recovery algorithm

Input: \mathbf{y} , $\epsilon = 10^{-6}$, max iterations (J), \mathbf{A}_l , \mathbf{A}_s .

Initialization: $\rho = 10^{-2}$, $\rho_o = 1.001$, $t = 0$,

$L^0 = \mathbf{0}_{M,N}$, $S^0 = \mathbf{0}_{M,N}$, $\mathbf{u}^0 = \mathbf{0}_K$.

while $\|\mathbf{A}_l \text{vec}(L) + \mathbf{A}_s \text{vec}(S) - \mathbf{y}\|_2^2 > \epsilon$ or $t < J$ **do**

Get all the elements of λ_{LT}^t by (24), then estimate L by,

$$L^{t+1} = \text{SVT}_{\lambda_{LT}^t} \left(\mathbf{A}_l^* \left(\mathbf{y} - \mathbf{A}_s \text{vec}(S^t) + \frac{1}{\rho} \mathbf{u}^t \right) \right).$$

Get all the elements of λ_{ST}^t by (21), then estimate S by,

$$S^{t+1} = \text{ST}_{\lambda_{ST}^t} \left(\mathbf{A}_s^* \left(\mathbf{y} - \mathbf{A}_l \text{vec}(L^{t+1}) + \frac{1}{\rho} \mathbf{u}^t \right) \right).$$

$$\mathbf{u}^{t+1} = \mathbf{u}^t + \rho (\mathbf{A}_s \text{vec}(S^{t+1}) + \mathbf{A}_l \text{vec}(L^{t+1}) - \mathbf{y}).$$

$\rho = \min(\rho_o \times \rho, \rho_m)$, and $t = t + 1$.

$L \leftarrow L^{t+1}$ and $S \leftarrow S^{t+1}$.

Output: L, S .

III. UNFOLDING ADMM BASED LOW-RANK PLUS SPARSE RECOVERY ALGORITHM

In this section, we are going to discuss the ADMM algorithm unfolding using a dense DNN. An iterative algorithm given in Algorithm 1 utilizes a sequence of steps to estimate the solution based on the ADMM steps given in (14), (15) and (10). Here, previous estimates are used in the next iteration. Thus, this kind of iterative algorithm can be considered as a recurrent neural network. The t -th iteration of the iterative algorithm is modeled as the t -th layer of the deep neural network. Each matrix multiplication given in the ADMM steps (14), (15) and (10) is considered as the weights of the deep neural network. Now, these matrix multiplications are implemented as linear layers i.e., a single matrix multiplication is implemented as a single linear layer without a bias. Here, our main objective is to learn the per iteration weights of the network and thresholding parameters λ_S and λ_L given in (21)

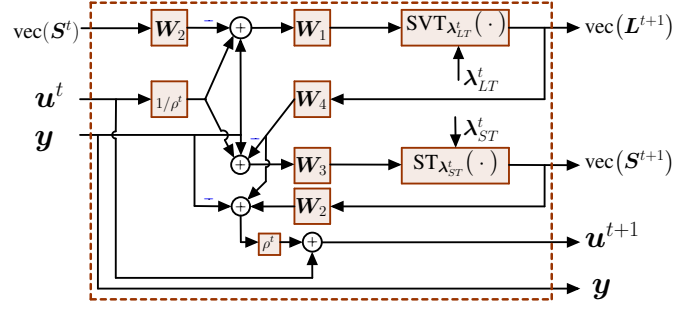


Fig. 2. Block diagram of the t -th layer of the DNN which mimic the low-rank plus sparse recovery Algorithm 1.

and (24) from the training data. To this end, the t -th layer of the neural network is represented by the following equations.

$$L^{t+1} = \text{SVT}_{\lambda_{LT}^t} \left(\mathbf{W}_1^t \left(\mathbf{y} - \mathbf{W}_2^t \text{vec}(S^t) + \frac{\mathbf{u}^t}{\rho^t} \right) \right), \quad (25)$$

$$S^{t+1} = \text{ST}_{\lambda_{ST}^t} \left(\mathbf{W}_3^t \left(\mathbf{y} - \mathbf{W}_4^t \text{vec}(L^{t+1}) + \frac{\mathbf{u}^t}{\rho^t} \right) \right), \quad (26)$$

$$\mathbf{u}^{t+1} = \mathbf{u}^t + \rho^t (\mathbf{W}_2^t \text{vec}(S^{t+1}) + \mathbf{W}_4^t \text{vec}(L^{t+1}) - \mathbf{y}). \quad (27)$$

Here, \mathbf{W}_1^t , \mathbf{W}_2^t , \mathbf{W}_3^t and \mathbf{W}_4^t are the weights of the t -th layer of the deep neural network as shown in Fig. 2, their initial values are $\mathbf{W}_1^t = \mathbf{A}_l^*$, $\mathbf{W}_2^t = \mathbf{A}_s$, $\mathbf{W}_3^t = \mathbf{A}_s^*$ and $\mathbf{W}_4^t = \mathbf{A}_l$ to mimic the ADMM Algorithm 1. Further, λ_{LT}^t and λ_{ST}^t are the thresholding vectors of the t -th layer as given in (14) and (15). Note that, λ_{LT}^t and λ_{ST}^t depend on the previous estimates of the L^t , S^t and two parameters (λ_S and λ_L). Here, we consider matrices \mathbf{W}_1^t , \mathbf{W}_2^t , \mathbf{W}_3^t and \mathbf{W}_4^t are tied over all the layers, i.e., sharing weights. However, we do not consider thresholding parameters (λ_S and λ_L) and γ to be tied over all layers, i.e., each layer has its own thresholding parameters. To this end, $\Theta = \{\lambda_S^t, \lambda_L^t, \gamma^t, \rho^t, \mathbf{W}_1, \mathbf{W}_2, \mathbf{W}_3, \mathbf{W}_4\}$ represents the set of learning parameters. Here, λ_S^t and λ_L^t are the thresholding parameters of the t -th layer. The unfolded architecture of the low-rank plus sparse recovery Algorithm 1 is shown in Fig. 2. Here, this figure shows a single layer of the deep neural network (t -th layer) and this layer is equivalent to the t -th iteration of Algorithm 1.

A. Training phase

In the training phase, the DNN is trained in a supervised manner. Here, the DNN learns the parameters given in $\Theta = \{\lambda_S^t, \lambda_L^t, \gamma^t, \rho^t, \mathbf{W}_1, \mathbf{W}_2, \mathbf{W}_3, \mathbf{W}_4\}$. Suppose that the DNN has T layers, then the outputs of the DNN in the training phase for the i -th sample are given by \hat{L}_i and \hat{S}_i , respectively. Note that, in the training phase, the DNN minimizes the normalized mean squared error

$$\text{MSE} = \frac{1}{T_s} \sum_{i=1}^{T_s} \left(\frac{1}{2} \frac{\|\hat{L}_i - L_i\|_F^2}{\|L_i\|_F^2} + \frac{1}{2} \frac{\|\hat{S}_i - S_i\|_F^2}{\|S_i\|_F^2} \right), \quad (28)$$

where S_i and L_i are i -th ground-truth low rank and sparse matrices and T_s is the number of training samples.

In this work, we consider three versions of the proposed DNN based ADMM thresholding as follows. (a) Parameter learning with non-adaptive thresholding (i.e., $g_s(x) = g_l(x) = 1$). This approach is named as ADMM based trained RPCA with thresholding (TRPCA-T). For the parameter learning with adaptive thresholding, we consider two versions based on two decay functions as described in II-D. These two approaches are named as follows. (b) ADMM based trained RPCA with adaptive thresholding based on logarithm heuristic (TRPCA-AT(log)). (c) ADMM based trained RPCA with adaptive thresholding based on exponential heuristic (TRPCA-AT(exp)).

To have a comparison with our proposed approach, we consider two approaches. In the first approach, we consider the untrained ADMM approach to solve the low-rank plus sparse recovery as given in Algorithm 1 with $g_s(x) = g_l(x) = 1$ (i.e., by using the ℓ_1 -norm and nuclear norm). This method is named as ADMM based untrained RPCA with thresholding (URPCA-T). As a second option, we consider the convex relaxation of the low-rank plus sparse recovery problem given in (7). This method is named as low-rank plus sparse recovery with convex relaxation (LRPSRC).

B. Computation complexity

In this sub-section, the computational complexity of the proposed DNN is discussed. Note that the t -th iteration of Algorithm 1 is shown in Fig. 2. Here, a single layer of the DNN consists of four dense linear layers and their weight matrices are given with $\mathbf{W}_1^t, \mathbf{W}_3^t \in \mathbb{C}^{K \times MN}$ and $\mathbf{W}_2^t, \mathbf{W}_4^t \in \mathbb{C}^{MN \times K}$. In the feed-forward propagation, data propagation is given in eqs. (25), (26) and (27). Now, for T_s number of training samples and n number of epochs, the computational complexity of the feed-forward propagation is $\mathcal{O}(6T_s n(MNK) + \mathcal{O}(T_s n(M^2N + MN^2 + N^3)) + \mathcal{O}(T_s n(M^2N + N^2M))) \approx \mathcal{O}(T_s n(MNK + M^2N + N^2M + N^3))$. When $M = N$, the computational complexity of the feed-forward propagation is given by $\mathcal{O}(T_s n(N^2K + N^3))$. Here, $\mathcal{O}(\cdot)$ is the Big O notation for asymptotic computational complexity analysis [42]. It is used to analyze the computational performance of an algorithm as input size increases. For the back propagation, the computational complexity of the linear layers is given by $\mathcal{O}(6T_s n(MNK))$ and for the back propagation through SVD it is given by $\mathcal{O}(T_s n(M^2N + MN^2 + N^3)) + \mathcal{O}(T_s n(M^2N + N^2M))$. Hence, the training complexity of the DNN is the addition of the feed-forward propagation and the back propagation complexities. Now, for $M = N$, the training complexity of the DNN is given by $\mathcal{O}(2T_s n(N^2K + N^3)) \approx \mathcal{O}(T_s n(N^2K + N^3))$. This computational complexity corresponds to the single iteration of Algorithm 1. Now, for T iterations/layers the training computational complexity is given by $\mathcal{O}(TT_s n(N^2K + N^3))$. The testing computational complexity is the feed-forward propagation complexity of the data through the DNN. It is given by $\mathcal{O}(TN_s(N^2K + N^3))$, here N_s is the number of testing samples.

IV. RESULTS

In this section numerical results are presented. First, the performance of deep learning-based trained ADMM adaptive thresholding is evaluated with a generic real-valued Gaussian model and next a complex-valued SFCW radar model given in Section II-A is used.

A. Generic Gaussian model

Here, the elements of the matrix $\mathbf{A}_l = \mathbf{A}_s = \mathbf{A} \in \mathbb{R}^{K \times MN}$ are generated once from an i.i.d. Gaussian distribution with zero mean and unit variance. \mathbf{y} is generated based on the (1). Further, we normalized the matrices \mathbf{S} and \mathbf{L} to have a unit Frobenius norm (i.e., $\|\mathbf{L}\|_F^2 = \|\mathbf{S}\|_F^2 = 1$). The signal-to-noise ratio is $\text{SNR} := \|\text{Avec}(\mathbf{L} + \mathbf{S})\|_2^2 / \|\mathbf{n}\|_2^2 = 20\text{dB}$ and $M = 30, N = 30$. Generally, many training samples are required to train a deep neural network. However, due to the specific architecture of the iterative algorithm, here we are able to train the DNN with a small data set of 500 samples. In the training phase, the adaptive moment estimation (Adam) optimizer [43] with a learning rate of 0.1 is used to train the DNN and batch size was set as 50. Note that, in the Gaussian model, the DNN only learns the λ_S^t and λ_L^t instead of all the parameters given in Θ . This is due to the fact that the performance gain improvement learning all the parameters given in Θ is very small compared to learning only λ_S^t and λ_L^t . Here, we initialize $\mathbf{W}_1^t = \mathbf{A}_l^\dagger, \mathbf{W}_2^t = \mathbf{A}_s, \mathbf{W}_3^t = \mathbf{A}_s^\dagger$ and $\mathbf{W}_4^t = \mathbf{A}_l$ to mimic the ADMM Algorithm 1 and $\gamma = 1$. The DNN is trained over a maximum of 500 epochs. In the inference phase, to evaluate the performance of the DNN, the normalized average root mean squared error is used. For low-rank and sparse matrix, it is given by

$$\text{RMSE}_L = \frac{1}{N_s} \sum_{i=1}^{N_s} \left(\frac{\|\hat{\mathbf{L}}_i - \mathbf{L}_i\|_F}{\|\mathbf{L}_i\|_F} \right), \quad (29)$$

$$\text{RMSE}_S = \frac{1}{N_s} \sum_{i=1}^{N_s} \left(\frac{\|\hat{\mathbf{S}}_i - \mathbf{S}_i\|_F}{\|\mathbf{S}_i\|_F} \right). \quad (30)$$

The CRB given in (3) is based on the combined recovery error of both low-rank and sparse matrices. Now, for that, first we vectorize the matrices \mathbf{L} and \mathbf{S} and next, we cascade them to generate a single vector. For the i -th ground truth and estimated low-rank and sparse matrices these vectors are given by $\mathbf{x}_i = [\text{vec}(\mathbf{L}_i)^T \text{vec}(\mathbf{S}_i)^T]^T$ and $\hat{\mathbf{x}}_i = [\text{vec}(\hat{\mathbf{L}}_i)^T \text{vec}(\hat{\mathbf{S}}_i)^T]^T$, respectively. Now, the combined average root mean squared error is given by

$$\text{RMSE}_{LS} = \frac{1}{N_s} \sum_{i=1}^{N_s} (\|\mathbf{x}_i - \hat{\mathbf{x}}_i\|_2). \quad (31)$$

The outputs of a DNN with T layers is for the i -th testing sample are given by $\hat{\mathbf{S}}_i$ and $\hat{\mathbf{L}}_i$, respectively. Here, \mathbf{S}_i and \mathbf{L}_i are i -th ground-truth low rank and sparse matrices and $N_s = 1200$ is the number of testing samples. In this work, training and testing data are synthetically generated based on the system model given in (1). Therefore, ground-truth low-rank and sparse matrices are available. In case only the

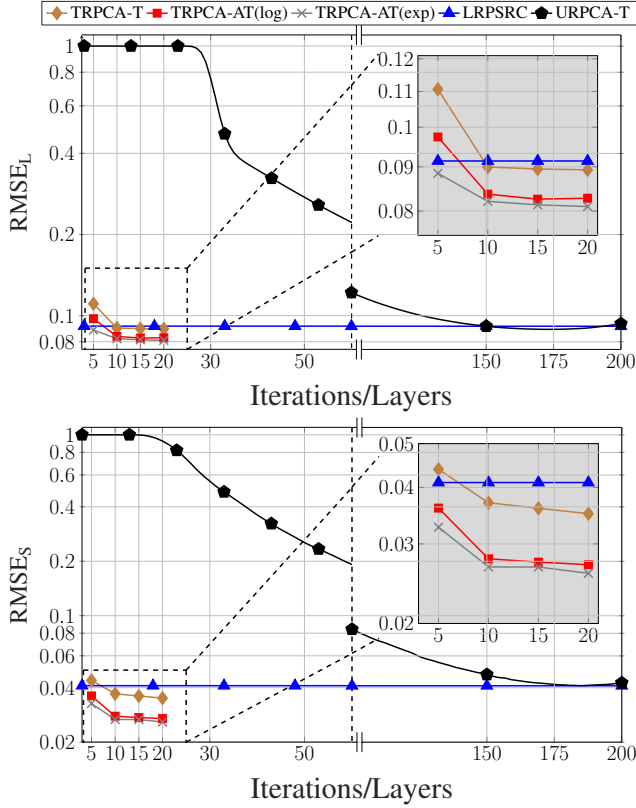


Fig. 3. Average recovery error of low-rank (top) and sparsity (bottom) contributions for compression ratio $K/MN = 50\%$.

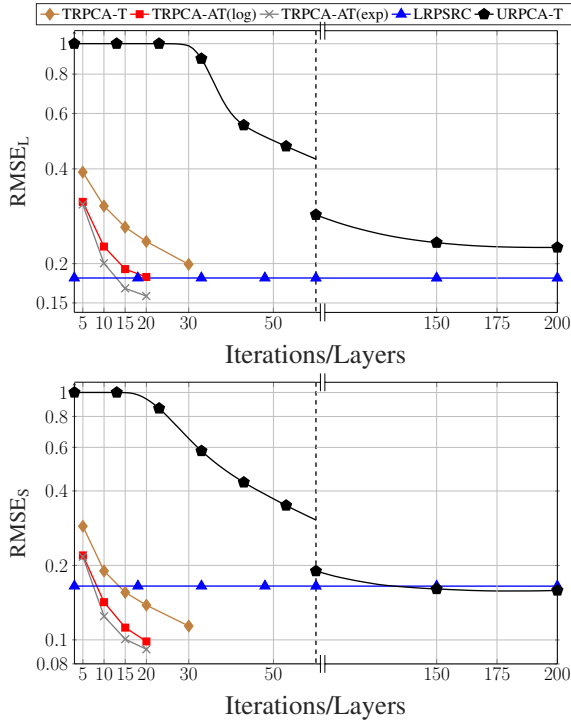


Fig. 4. Average recovery error of low-rank (top) and sparsity (bottom) contributions for compression ratio $K/MN = 25\%$.

received data vector \mathbf{y} in (1) is available, Algorithm 1 can be used to generate ground-truth low-rank and sparse matrices.

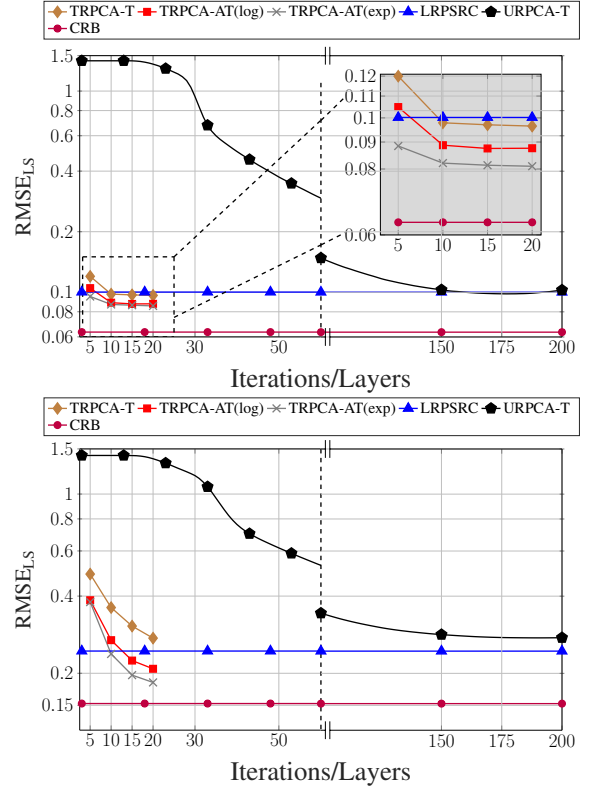


Fig. 5. Average combined recovery error of low-rank and sparse matrices given in (31) for compression ratio $K/MN = 50\%$ (top) and $K/MN = 25\%$ (bottom).

Both Algorithm 1 and LRPSRC given in (7) are implemented using Matlab [44] and LRPSRC is solved using the CVX package [45]. Notice that, in the LRPSRC λ_l and λ_s are set to 1, and $1/\sqrt{\max(M, N)}$, respectively as suggested by [13]. Note that for Algorithm 1, there is no specific rule to select the λ_l and λ_s and ρ , thus they are manually tuned based on the data³. Note that as a rule of thumb, thresholding parameters λ_S and λ_L given in (21) and (24) are initialized as $\lambda_S = \lambda_s/\rho$ and $\lambda_L = \lambda_l/\rho$, respectively [13]. The Pytorch package is used to implement the DNN [46].

The average normalized RMSEs for the different number of layers of the DNN are for compression ratio (K/MN) 50% and 25% shown in Figs. 3 and 4, respectively. Figs. 3 and 4 show that the proposed DNN based thresholding (TRPCA-AT(log) and TRPCA-AT(exp)) outperforms the URPCA-T and the LRPSRC. Further, it is observed that as the number of layers increases the average RMSE decreases. For the 50% compressing ratio, the average RMSE does not show a large variance after ten layers. However, for the 25% compressing ratio this is not the case. This is due to the fact that, as the compression ratio increases recovering of the low-rank and the sparse matrices become more challenging.

Further, the TRPCA-AT outperforms the TRPCA-T. This performance improvement is mainly due to the iterative reweighting of ℓ_1 -norm and nuclear norm minimization. Also, the improvement over non-weighting to iterative reweighting

³When \mathbf{A} is identity matrix, there is a specific rule to select λ_s as $1/\sqrt{\max(M, N)}$ [13].

is more visible as the compression ratio increases (i.e., as the problem getting more challenging). As an example, for the 25% compressing ratio, the average RMSE improvement between the TRPCA-T with twenty layers and TRPCA-AT(exp) with twenty layers for the low-rank and sparse components are 32.93% and 50.77%, respectively. However, for the 50% compressing ratio, this improvement for the low-rank and sparse components are 9.31% and 26.21%, respectively. Further, we observe slight performance gains as the decay function is changed from log-determinant to exponential. As we compare the number of layers of the TRPCA-AT to the number of iterations of the URPCA-T, the TRPCA-AT achieves 1 : 20 improvement. In more details, TRPCA-AT with ten layers outperforms URPCA-T with 200 iterations. Therefore, in the testing phase (inference phase), our proposed approach (TRPCA-AT) is twenty times faster than the conventional untrained approach (URPCA-T).

Fig. 5 shows the CRB of the combined low-rank and sparse matrices estimation for compression ratios 50% and 25%. It can be seen that the non-convex approach TRPCA-AT has the closest performance to the CRB. As the compression ratio increases, the estimation of low-rank and sparse matrices from compressive measurements becomes more challenging. This can be seen as the compression ratio changes from 50% to 25% the CRB has increased.

B. SFCW radar model

In this subsection, the performance evaluation of the ADMM based trained RPCA with adaptive thresholding was performed based on the SFCW radar model given in Section II-A. In the simulations, we set the carrier frequency f_c of 300 GHz and bandwidth B as 5 GHz. Further, both N and M are set as 30. The inter-antenna spacing is chosen as half of the wavelength of f_c . Here, we consider a single-layered structure and the distance to the front surface of the layered structure is 1.0 m. Both height and length of the layered structure is 0.5 m. In the simulations, we consider six defects and the scene is partitioned into a 16×16 grid with equal grid size (i.e., $Q = 256$). The grid size is selected according to the Rayleigh resolution of the radar. In the simulations, the signal-to-noise ratio is $\text{SNR} := \|\Phi \text{vec}(\mathbf{Y}^t) + \Phi \mathbf{D} \mathbf{s}\|_2^2 / \|\Phi \text{vec}(\mathbf{Z})\|_2^2 = 20\text{dB}$. Note that the SFCW data consists of complex numbers, thus, in this work, we implemented the DNN which supports complex numbers by using the PyTorch version 1.8.1. Here, we initialize $\mathbf{W}_1^t = \mathbf{A}_l^H$, $\mathbf{W}_2^t = \mathbf{A}_s$, $\mathbf{W}_3^t = \mathbf{A}_s^H$ and $\mathbf{W}_4^t = \mathbf{A}_l$ to mimic the ADMM Algorithm 1.

Interestingly, in contrast to the generic Gaussian model only learning the λ_S^t and λ_L^t does not achieve satisfactory average RMSEs of the low-rank and sparse components. Therefore, we enable learning all parameters given in Θ . Further, we notice that the stochastic gradient descent (SGD) optimizer [47] performs better than the Adam optimizer in learning all the parameters given in Θ together. Therefore, we consider a three-stage training process for better learning.

In the first stage, we only learn the λ_S^t and λ_L^t for 50 epochs using the Adam optimizer. In the second stage, we learn all parameters given in Θ using the SGD optimizer for 50 epochs.

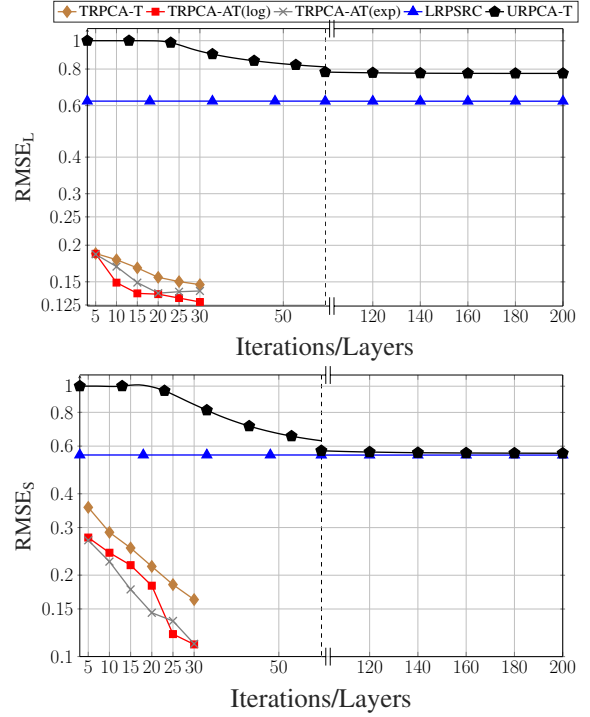


Fig. 6. Average RMSE of low-rank (top) and sparsity (bottom) contributions for $K/M/N = 20\%$ for SFCW model.

Finally, we only learn the λ_S^t and λ_L^t for 15 epochs using the Adam optimizer. Also, we slightly adjusted the learning rate as the number of layers of the DNN increases. For the first stage, we employed learning rates 1×10^{-1} , 5×10^{-2} and 5×10^{-3} for the DNN with 5/10, 15/20 and 25/30 layers, respectively. Here, only exception is the TRPCA-T. For the TRPCA-T, we consider the learning rate of 5×10^{-2} for the DNN with 25/30 layers as well. This is due to the fact that, the non-adaptive thresholding based TRPCA-T is less sensitive to the change of parameters compared to the adaptive thresholding based TRPCA-AT. For the second and third stages, we employed the learning rates 1×10^{-3} , 2.5×10^{-4} for all layers combinations of the DNN, respectively. The main reason to consider the third training stage is that, it achieves higher performance gains with respect to continuation of the second training stage for another 15 epochs. Also, note that there is a specific reason to use the first stage without directly using the second stage. This is due to the unbalance of \mathbf{A}_s and \mathbf{A}_l of the SFCW model compared to the generic Gaussian model. Note that, $\mathbf{A}_s = \Phi \mathbf{D}$ and $\mathbf{A}_l = \Phi$. More specifically, $\mathbf{A}_l = \Phi$ and Φ is the selection matrix. This matrix has a single non-zero element of value 1 in each row to indicate the selected frequency of a particular antenna if that antenna is selected. However, $\mathbf{A}_s = \Phi \mathbf{D}$ so, \mathbf{A}_s is a combination of the selection matrix and the matrix \mathbf{D} . Note that, the matrix \mathbf{D} is generated based on the time delays of the grid (as described in Section II-A). Therefore, the matrix \mathbf{A}_s contains more information compared to the matrix \mathbf{A}_l . Therefore, \mathbf{A}_s is more difficult to learn compared to \mathbf{A}_l . This results in an imbalance in the training phase if we directly start with the stage two. That means the RMSE of the low-rank component tends to be much smaller

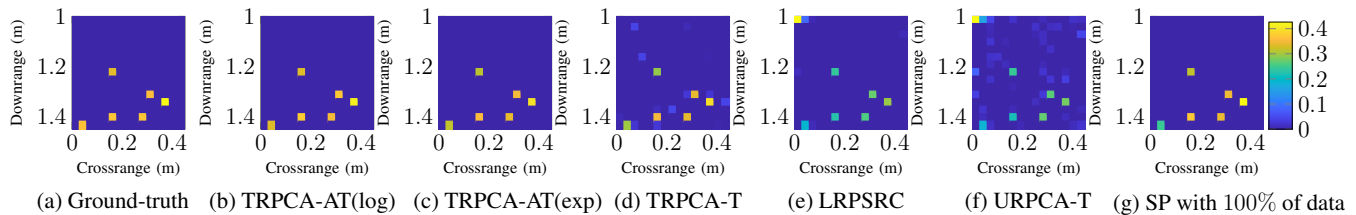


Fig. 7. Object recovery in single case for compression ratio $K/MN = 20\%$

compared to the RMSE of the sparse component in the training phase if we directly start with the second stage.

In the defect detection by SFCW radar, we consider a data set of 600 samples. Here, 500 data samples are used for training and validation and 100 data samples are used for testing. Here, we used Matlab [44] to generate the SFCW data based on the system model given in (6). The average normalized RMSEs for the different numbers of layers of the DNN for the compression ratio (K/MN) 20% is shown in Fig. 6. The figure shows that the proposed TRPCA-AT outperforms both URPCA-T and the LRPSRC given in (7). Further, in terms of the average RMSE, the TRPCA-AT and TRPCA-T with five layers outperform URPCA-T with 200 iterations. Therefore, as we compare the number of layers of the TRPCA-AT to the number of iterations of the URPCA-T, the TRPCA-AT achieves an 1 : 40 improvement for the SFCW radar data, i.e., our proposed approach (TRPCA-AT) is forty times faster than the conventional untrained approach (URPCA-T). Moreover, based on the results shown in Fig. 6, the TRPCA-AT shows better performance compared to the TRPCA-T. Also, note that with 20% compression ratio, the estimation of \mathbf{Y}^l and \mathbf{s} from \mathbf{y}_{cs} in (6) is more challenging. Therefore, the average RMSE of the LRPSRC is higher than 0.5. However, the DNN based TRPCA-AT is able to achieve average RMSE in the range of 0.1 for both sparse and the low-rank components. Since the matrices \mathbf{A}_s and \mathbf{A}_l are unequal in the SFCW radar model, we did not consider the CRB benchmark given in (3).

Next, to further illustrate the defect detection, an image of the recovered detects are formed. Here, the recovered vector \mathbf{s} is reshaped into a matrix to obtain an image of the detects as shown in Fig. 7 for a single data sample. As a benchmark here we consider the state-of-the-art subspace projection (SP) [11] method with the full data set (i.e., compression ratio (K/MN) = 100%). Further, for SP, it is assumed that the number of defects is known. Fig. 7 (a) shows the actual defect locations. The recovered locations of the defects for the ADMM based trained RPCA with adaptive thresholding based on logarithm heuristic (TRPCA-AT(log)), ADMM based trained RPCA with adaptive thresholding based on exponential heuristic (TRPCA-AT(exp)), ADMM based trained RPCA with thresholding (TRPCA-T), the LRPSRC, ADMM based untrained RPCA with thresholding (URPCA-T) and the SP are shown in Fig. 7 (b), (c), (d), (e), (f) and (g), respectively. It can be seen that the proposed TRPCA-AT approaches are able to identify all six defects. Further, the proposed TRPCA-AT approaches are able to estimate amplitudes of the recovered

defects (vector \mathbf{s}) closer to the actual defects. Therefore, it is observed that defect detection with the proposed TRPCA-AT approaches outperform state-of-the-art SP even with 20% of data.

V. CONCLUSION

This paper presents a deep learning-based low-rank plus sparse recovery approach for the detection of material defects based on compressive sensing. To this end, an iterative algorithm is developed based on ADMM to estimate the low-rank and sparse contributions with the iterative reweighted nuclear and ℓ_1 -norm minimization. In particular, we propose deep learning based algorithm unfolding to improve the accuracies of the recovered low-rank and sparse components and the speed of convergence of the algorithm. The results show that, the deep learning based algorithm unfolding performs substantially better compared to the untrained iterative algorithm in terms of low-rank and sparse component recovery and convergence speed. In addition to that, it is observed that as the compression ratio increases, the improvement with deep learning becomes more visible.

REFERENCES

- [1] S. Gholizadeh, "A review of non-destructive testing methods of composite materials," *Procedia Structural Integrity*, vol. 1, pp. 50–57, 2016.
- [2] P. Hillger, M. van Delden, U. S. Miriya Thantrige, A. M. Ahmed, J. Witteimer, K. Arzi, M. Andree, B. Sievert, W. Prost, A. Rennings, D. Erni, T. Musch, N. Weimann, A. Sezgin, N. Pohl, and U. R. Pfeiffer, "Toward mobile integrated electronic systems at THz frequencies," *J. Infrared Millim. Terahertz Waves*, vol. 41, no. 7, pp. 846–869, 2020.
- [3] A. Chopard, J. B. Sleiman, Q. Cassar, J. Guillet, M. Pan, J. Perraud, A. Susset, and P. Mounaix, "Terahertz waves for contactless control and imaging in aeronautics industry," *NDT & E International*, vol. 122, p. 102473, 2021.
- [4] V. H. Tang, A. Bouzerdoum, and S. L. Phung, "Multipolarization through-wall radar imaging using low-rank and jointly-sparse representations," *IEEE Trans. on Image Process.*, vol. 27, no. 4, pp. 1763–1776, 2018.
- [5] A. Kariminezhad and A. Sezgin, "Spatio-temporal waveform design in active sensing systems with multilayer targets," in *EUSIPCO*, 2019, pp. 1–5.
- [6] U. S. K. P. Miriya Thantrige, J. Barowski, I. Rolfes, D. Erni, T. Kaiser, and A. Sezgin, "Characterization of dielectric materials by sparse signal processing with iterative dictionary updates," *IEEE Sens. Lett.*, vol. 4, no. 9, pp. 1–4, 2020.
- [7] O. Zahran, H. Kasban, M. El-Kordy, and F. Abd El-Samie, "Automatic weld defect identification from radiographic images," *NDT & E International*, vol. 57, pp. 26–35, 2013.
- [8] C. D. Stoik, M. J. Bohn, and J. L. Blackshire, "Nondestructive evaluation of aircraft composites using transmissive Terahertz time domain spectroscopy," *Optics express*, vol. 16, no. 21, pp. 17 039–17 051, 2008.
- [9] S. Unnikrishnakurup, J. Dash, S. Ray, B. Pesala, and K. Balasubramaniam, "Nondestructive evaluation of thermal barrier coating thickness degradation using pulsed IR thermography and THz-TDS measurements: A comparative study," *NDT & E International*, vol. 116, p. 102367, 2020.

- [10] Q. Huang, L. Qu, B. Wu, and G. Fang, "UWB through-wall imaging based on compressive sensing," *IEEE Trans. on Geosci. and Remote Sensing*, vol. 48, no. 3, pp. 1408–1415, 2010.
- [11] U. S. Khan and W. Al-Nuaimy, "Background removal from GPR data using eigenvalues," in *Proc. of the XIII Int. Conf. on Ground Penetrating Radar*, 2010, pp. 1–5.
- [12] D. L. Donoho, "Compressed sensing," *IEEE Trans. Inf. Theory*, vol. 52, no. 4, pp. 1289–1306, 2006.
- [13] E. J. Candès, X. Li, Y. Ma, and J. Wright, "Robust principal component analysis?" *Journal of the ACM*, vol. 58, no. 3, pp. 1–37, 2011.
- [14] G. Tang and A. Nehorai, "Constrained cramer–rao bound on robust principal component analysis," *IEEE Trans. on Signal Process.*, vol. 59, no. 10, pp. 5070–5076, 2011.
- [15] A. M. Bruckstein, D. L. Donoho, and M. Elad, "From sparse solutions of systems of equations to sparse modeling of signals and images," *SIAM Review*, vol. 51, no. 1, pp. 34–81, 2009.
- [16] J. F. Cai, E. J. Candès, and Z. Shen, "A singular value thresholding algorithm for matrix completion," *SIAM Journal on Optimization*, vol. 20, no. 4, pp. 1956–1982, 2010.
- [17] M. Fazel, H. Hindi, and S. P. Boyd, "A rank minimization heuristic with application to minimum order system approximation," in *Proc. of the 2001 American Control Conf.*, vol. 6, 2001, pp. 4734–4739.
- [18] E. J. Candès and B. Recht, "Exact matrix completion via convex optimization," *Foundations of Computational mathematics*, vol. 9, no. 6, pp. 717–772, 2009.
- [19] D. Gross, "Recovering low-rank matrices from few coefficients in any basis," *IEEE Trans. Inf. Theory*, vol. 57, no. 3, pp. 1548–1566, 2011.
- [20] E. J. Candès and T. Tao, "The power of convex relaxation: Near-optimal matrix completion," *IEEE Trans. Inf. Theory*, vol. 56, no. 5, pp. 2053–2080, 2010.
- [21] E. J. Candès, M. B. Wakin, and S. P. Boyd, "Enhancing sparsity by reweighted ℓ_1 minimization," *Journal of Fourier analysis and Applications*, vol. 14, no. 5-6, pp. 877–905, 2008.
- [22] K. Mohan and M. Fazel, "Reweighted Nuclear norm minimization with application to system identification," in *Proc. of the 2010 American Control Conf.*, 2010, pp. 2953–2959.
- [23] S. Gu, Q. Xie, D. Meng, W. Zuo, X. Feng, and L. Zhang, "Weighted Nuclear norm minimization and its applications to low level vision," *Int. Journal of Comput. Vision*, vol. 121, no. 2, pp. 183–208, 2017.
- [24] I. Daubechies, R. DeVore, M. Fornasier, and C. S. Güntürk, "Iteratively reweighted least squares minimization for sparse recovery," *Communications on Pure and Applied Mathematics: A Journal Issued by the Courant Institute of Mathematical Sciences*, vol. 63, no. 1, pp. 1–38, 2010.
- [25] Y.-B. Zhao and D. Li, "Reweighted ℓ_1 -minimization for sparse solutions to underdetermined linear systems," *SIAM Journal on Optimization*, vol. 22, no. 3, pp. 1065–1088, 2012.
- [26] C. Lu, J. Feng, S. Yan, and Z. Lin, "A unified alternating direction method of multipliers by majorization minimization," *IEEE Trans. Pattern Anal. Mach. Intell.*, vol. 40, no. 3, pp. 527–541, 2018.
- [27] K. Gregor and Y. LeCun, "Learning fast approximations of sparse coding," in *Proc. of the 27th int. Conf. on Machine Learning*, 2010, pp. 399–406.
- [28] D. Kim and D. Park, "Element-wise adaptive thresholds for learned iterative shrinkage thresholding algorithms," *IEEE Access*, vol. 8, pp. 45 874–45 886, 2020.
- [29] O. Musa, P. Jung, and G. Caire, "Plug-and-play learned Gaussian-mixture approximate message passing," in *ICASSP*, 2021, pp. 4855–4859.
- [30] Y. Li, M. Tofighi, J. Geng, V. Monga, and Y. C. Eldar, "Efficient and interpretable deep blind image deblurring via algorithm unrolling," *IEEE Trans. Comput. Imag.*, vol. 6, pp. 666–681, 2020.
- [31] V. Monga, Y. Li, and Y. C. Eldar, "Algorithm unrolling: Interpretable, efficient deep learning for signal and image processing," *IEEE Signal Process. Magazine*, vol. 38, no. 2, pp. 18–44, 2021.
- [32] S. Gu, L. Zhang, W. Zuo, and X. Feng, "Weighted Nuclear norm minimization with application to image denoising," in *Proc. of the IEEE Conf. on Comput. Vision and Pattern Recognition*, 2014, pp. 2862–2869.
- [33] O. Solomon, R. Cohen, Y. Zhang, Y. Yang, Q. He, J. Luo, R. J. G. van Sloun, and Y. C. Eldar, "Deep unfolded robust PCA with application to clutter suppression in ultrasound," *IEEE Trans. Med. Imag.*, vol. 39, no. 4, pp. 1051–1063, 2020.
- [34] R. Cohen, Y. Zhang, O. Solomon, D. Toberman, L. Taieb, R. J. van Sloun, and Y. C. Eldar, "Deep convolutional robust PCA with application to ultrasound imaging," in *ICASSP*, 2019, pp. 3212–3216.
- [35] X. Yuan and J. Yang, "Sparse and low-rank matrix decomposition via alternating direction methods," *preprint*, vol. 12, no. 2, 2009.
- [36] S. Tao, D. Boley, and S. Zhang, "Convergence of common proximal methods for L1-regularized least squares," in *Twenty-Fourth Int. Joint Conf. on Artificial Intelligence*, 2015.
- [37] D. Wipf and S. Nagarajan, "Iterative reweighted ℓ_1 and ℓ_2 methods for finding sparse solutions," *IEEE J. Sel. Topics Signal Process.*, vol. 4, no. 2, pp. 317–329, 2010.
- [38] M. Malek-Mohammadi, M. Babaie-Zadeh, and M. Skoglund, "Iterative concave rank approximation for recovering low-rank matrices," *IEEE Trans. on Signal Process.*, vol. 62, no. 20, pp. 5213–5226, 2014.
- [39] M. Fazel, H. Hindi, and S. P. Boyd, "Log-det heuristic for matrix rank minimization with applications to Hankel and Euclidean distance matrices," in *Proc. of the 2003 American Control Conf., 2003.*, vol. 3, 2003, pp. 2156–2162 vol.3.
- [40] C. Lu, J. Tang, S. Yan, and Z. Lin, "Nonconvex nonsmooth low rank minimization via iteratively reweighted Nuclear norm," *IEEE Trans. on Image Process.*, vol. 25, no. 2, pp. 829–839, 2016.
- [41] Y. Peng, J. Suo, Q. Dai, and W. Xu, "Reweighted low-rank matrix recovery and its application in image restoration," *IEEE Trans. on Cybernetics*, vol. 44, no. 12, pp. 2418–2430, 2014.
- [42] I. Chivers and J. Sleightholme, "An introduction to algorithms and the big o notation," in *Introduction to programming with Fortran*. Springer, 2015, pp. 359–364.
- [43] D. P. Kingma and J. Ba, "Adam: A Method for Stochastic Optimization," *arXiv preprint arXiv:1412.6980*, 2017.
- [44] The MathWorks Inc, *MATLAB: version 9.6.0 (R2019a)*, 2019.
- [45] M. Grant and S. Boyd, *CVX: Matlab Software for Disciplined Convex Programming, version 2.1*, Mar. 2014.
- [46] A. Paszke et al., "Pytorch: An imperative style, high-performance deep learning library," *Advances in Neural Information Processing Systems* 32, pp. 8024–8035, 2019.
- [47] I. Sutskever, J. Martens, G. Dahl, and G. Hinton, "On the importance of initialization and momentum in deep learning," in *Int. Conf. on Machine Learning*, 2013, pp. 1139–1147.